Supporting Information

Hybrid Anatase/Rutile Nanodots-Embedded Covalent Organic Frameworks with Complementary Polysulfide Adsorption for High-Performance Lithium–Sulfur Batteries

Ziyi Yang,[†,‡,▽] Chengxin Peng,[‡,§,▽] Ruijin Meng,[†,‡,▽] Lianhai Zu,[†] Yutong Feng,[†] Bingjie Chen,[†] Yongli Mi,[⊥] Chi Zhang,[†,‡,] and Jinhu Yang,[†,‡,*]*

[†] School of Chemical Science and Engineering, Tongji University, Shanghai, 200092, China [‡] Research Center for Translational Medicine and Key Laboratory of Arrhythmias of the Ministry of Education of China, East Hospital Tongji University School of Medicine, No. 150 Jimo Road, Shanghai, 200120, China

[§] School of Materials Science and Engineering, University of Shanghai for Science and Technology, Shanghai, 200093,China

⊥ Department of Chemical and Biomolecular Engineering, The Hong Kong University of Science and Technology, Clear Water Bay, Kowloon, Hong Kong, China

EXPERIMENTAL METODES

Chemicals and Materials. 1, 4-Dicyanobenzene (DCB) was purchased from Sigma-Aldrich (Mainland, China). Titanium (IV) butoxide (TBOT) was purchased from Sigma Chemical Co. (St. Louis, Mo). Zinc chloride (ABCR, anhydrous, 98 %), Tetrahydrofuran (THF), acetonitrile and N-Methyl-2-pyrrolidone were purchased from Aladdin Biological Technology Co., LTD (China). Borosilicate glass ampoule was purchased from AS-ONE Co., LTD (JP).

Preparation of the HCPT@COF composites. In a typical preparation, 500 mg of DCB powder was dispersed in 25.0 mL of N-Methyl-2-pyrrolidone (NMP)-ethanol mixture (v : v = 1:3) under rigorous sonication followed by adding 250 μL TBOT into the dispersion. After 4 h of sonication, 0.05 mL of deionized water was added dropwise to the dispersion under continuously stirring for 6.0 h. The resulting suspension was filtrated, washed with ethanol, collected and dried in a vacuum oven at 60 ^{o}C for 12 h, resulting in white powder of DCB@$Ti(OH)_4$.

The as-prepared DCB@$Ti(OH)_4$ powder was mixed with 200 mg catalyst of zinc chloride and transferred to a borosilicate glass ampoule. Then the ampoule was sealed under vacuum and kept at 400 ^{o}C for 20 h, leading to a black bulk product. The formed black bulk product was carefully taken out and grounded into powder. Finally, the product was washed successively with water, diluted HCl, THF and acetonitrile, followed by vacuum drying at 150 ^{o}C for further use. The

typical HCPT@COF composite with a thermolysis/polymerization temperature of 400 °C was also denoted as HCPT@COF-400. Moreover, the TiO_2@COF composites obtained at higher thermolysis/polymerization temperatures (500 and 700 °C) with otherwise conditions being typical were also prepared and denoted as TiO_2@COF-500 and TiO_2@COF-700 for comparisons.

Synthesis of TiO_2@COF/S composites. TiO_2@COF/S composites was prepared by the melt-diffusion strategy. Specifically, sulfur and TiO_2@COF composites were ball-milled in a mortar in a mass ratio of 80:20 and then transferred into an ampoule. The ampoule was then evacuated, sealed and heated at 155 °C for 10 h under Ar gas. To remove sulfur on the surface of the composite, the sample was treated for another two hours at the same temperature. The HCPT@COF/S composite and the COF/S composite hold an initial sulfur content of 69.3% and 70.1%, respectively, based on the TGA measurements.

Characterizations. The crystal structures and morphologies of the as-synthesized composites were characterized by powder X-ray diffraction (XRD, Rigaku D/max-2500 X-ray generator, Cu Kα radiation), field-emission scanning electron microscopy (SEM, FEI NanoSEM-430, 10 kV), transmission electron microscopy (TEM), and high-resolution transmission electron microscopy (HRTEM, Philips TecnaiF20, 200 kV) associated with energy-dispersive X-ray spectroscopy (EDS). X-ray photoelectron spectroscopy (XPS) investigations were conducted in a PHI-5000C ESCA system (PerkinElmer) with Mg Kαradiation ($\hbar\nu$= 1253.6 eV). X-ray photoelectron spectroscopy (XPS) spectra were measured with a constant analyzer pass energy of 46.95 eV. All binding energies (BEs) were referred to the C $_{1s}$ peak (284.6 eV). Gaussian-Lorentzian (20 % Gaussian) model was applied to the raw spectra to extract the peak positions. N_2

adsorption−desorption isotherms were collected on an Autosorb apparatus analyzer at 77 K. The Brunauer− Emmett−Teller method was utilized to calculate the surface areas over a P/P_0 range as described. NLDFT pore size distributions were determined using the silica/cylindrical pore model of the Quadrawin software. TGA analyses were carried out on a Netzsch TG209F1 apparatus at 10 K min-1 under N_2 atmosphere.

Electrochemical measurements. The electrode slurry was prepared by mixing TiO_2@COF/S composites, acetylene black and polyvinyldifluoride (PVDF) with a mass ratio of 70:20:10 in N-methylpyrrolidone (NMP) solvent. The slurry was then coated onto aluminum foil and vacuum dried at 60 ^oC for 12 h, giving rise to an average sulfur loading of about 1.2 mg cm^{-2}. Coin cells (type CR-2032) were fabricated in an Ar-filled glove box using Celgard 2400 polypropylene as the separator, lithium foil as the anode and 1.0 M lithium bis-trifluoromethanesulfonimide (LITFSI) as the electrolyte with 2 % $LiNO_3$ in tetraethylene glycol dimethyl ether (TEGDME) as the solvent. Galvanostatic discharge/charge tests were carried out using a LAND electric workstation (Wuhan LAND electronics Co., China) under a voltage range of 1.7-2.8 V. The specific capacities were calculated based on the weight of sulfur in the cathodes. Cyclic voltammetric measurements were carried out at a scan rate of 0.1 mV s^{-1} and EIS was conducted with

scanning frequency from 0.01 Hz to 100 kHz using a Solatron 1260/1287 Electrochemical Interface (Solatron Metrology, UK).

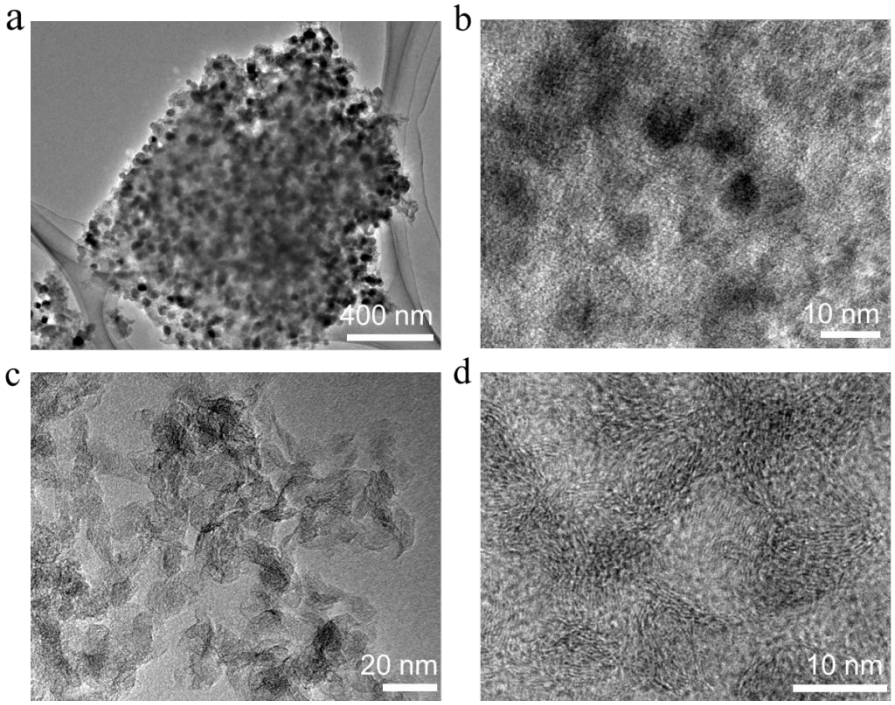

Figure S1. TEM images of the HCPT@COF composite prepared at 400 °C (a-b) and bare COF (c-d).

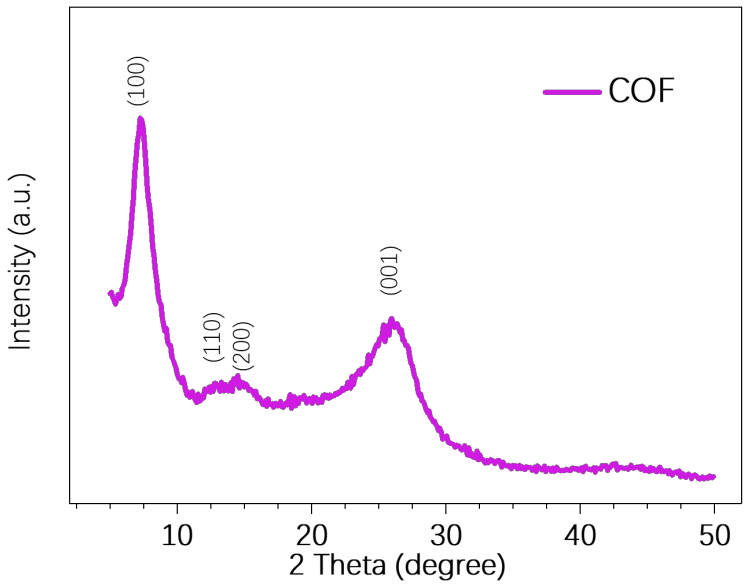

Figure S2. X-ray Diffraction pattern of bare COF synthesized at 400 °C

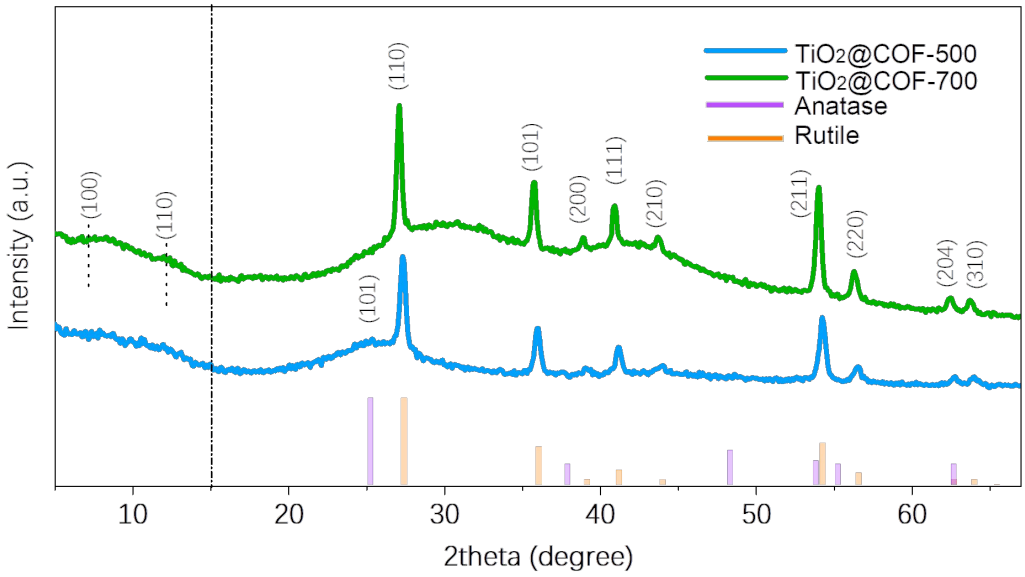

Figure S3. X-ray Diffraction patterns of TiO_2@COF composites synthesized at 500 and 700 °C.

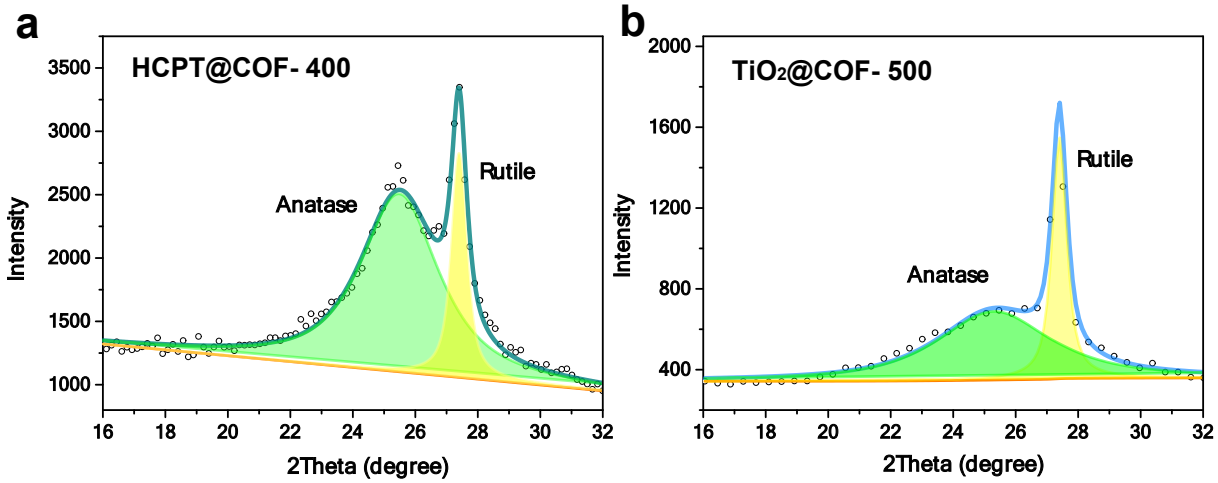

Figure S4. X-ray Diffraction peak fittings of the HCPT@COF composite prepared at 400 °C (a) and TiO_2@COF -500 °C (b).

Note: The XRD data were analyzed by "adiabatic analysis", and the ratios of rutile in TiO_2 was calculated by formula (1). The mass ratios of rutile to TiO_2 are 19.1 wt% and 39.6 wt% for HCPT@COF-400 and TiO_2@COF-500, respectively.

$$W_r = \frac{I_r}{I_r + \frac{I_a}{K_r^a}} \qquad (1)$$

W_r is the mass fraction of rutile phase TiO_2; I_r, I_a is the integrated intensity of the strongest peak of rutile and anatase, respectively; K_r^a is the RIR value (provided by the PDF standard card) of anatase divided by the RIR value of rutile, which is 3.3/3.4.

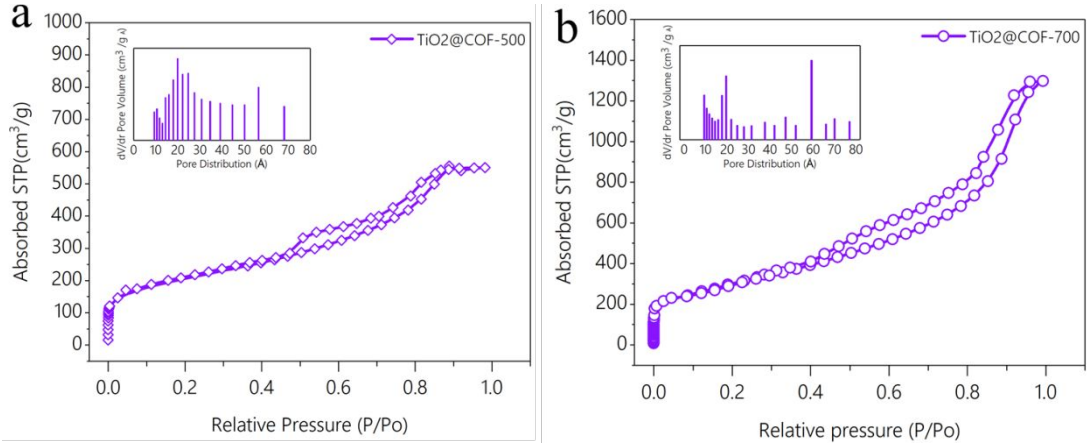

Figure S5. N_2 adsorption-desorption isotherms and the corresponding pore-size distribution diagrams (insets) of TiO_2@COF composites synthesized at 500 (a) and 700 ^oC (b).

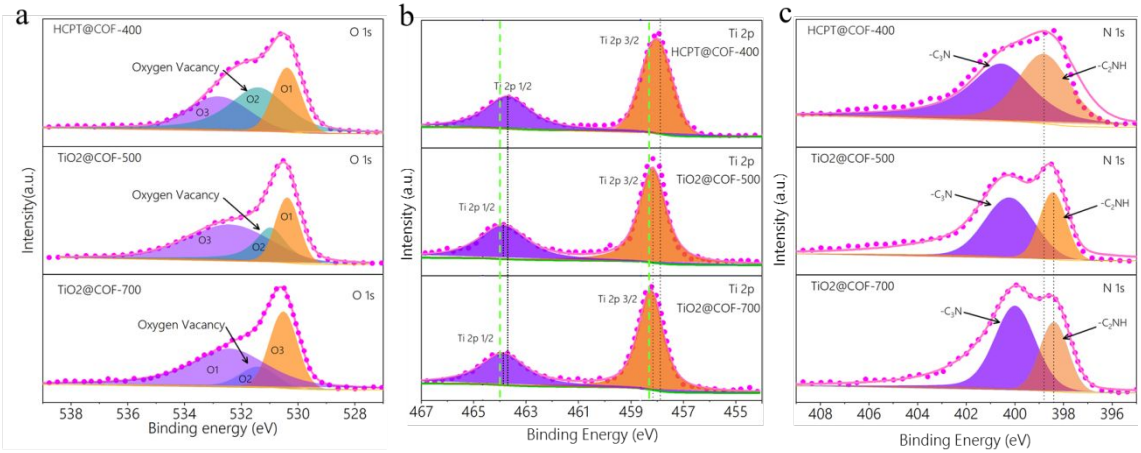

Figure S6. X-ray photoelectron spectra comparisons between TiO_2@COF composites synthesized at 400, 500 and 700 °C. (a) O *1s* spectra. (b) Ti *2p* spectra. (c) N *1s* spectra. Noted that the TiO_2@COF composite synthesized at 400°C (denoted as TiO_2@COF-400) corresponds to the typical sample of the HCPT@COF. Green vertical dotted lines in (b) correspond to the Ti *2p* binding energy of normal pure-phase TiO_2 without any heteroatom doped or other phase combined.

Note: O *1s* XPS spectrum (Figure S6a) shows that the peak induced by oxygen vacancy at ~531.5 eV drops, indicating the gradual disappearance of oxygen vacancy with increasing the reaction temperature. In addition, it is found that the binding energy of Ti *2p* increases, shifting to the position of Ti *2p* in normal TiO_2 (~ 464 eV, Figure S6b), while

the binding energy of N *1s* decreases, shifting to the position of N *1s* in bare COF (Figure S6c). Such a trend implies that the weakened interaction of N-Ti bonds between the two components of COF and TiO_2 at the higher temperatures. It can be deduced that the oxygen defects in the composite facilitate the formation of N-Ti bonds and the interaction of the two components.

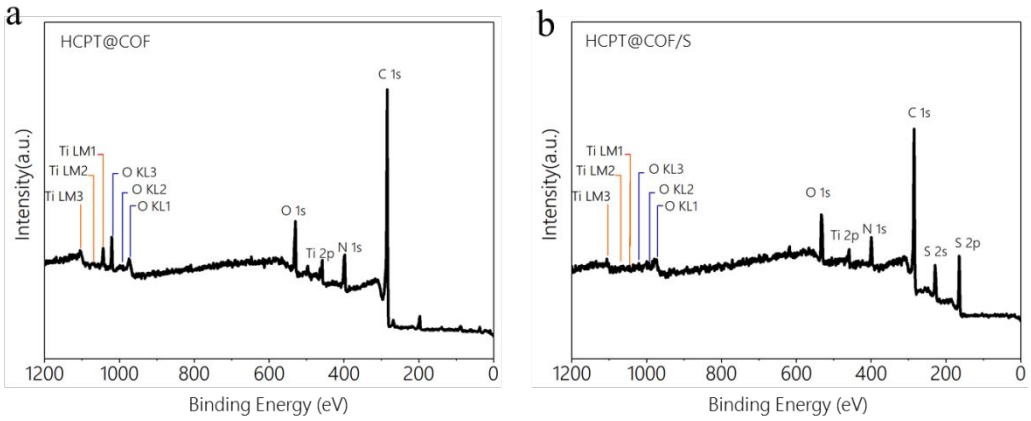

Figure S7. X-ray photoelectron overall spectra of the HCPT@COF composite (a) and the HCPT@COF/S composite (b).

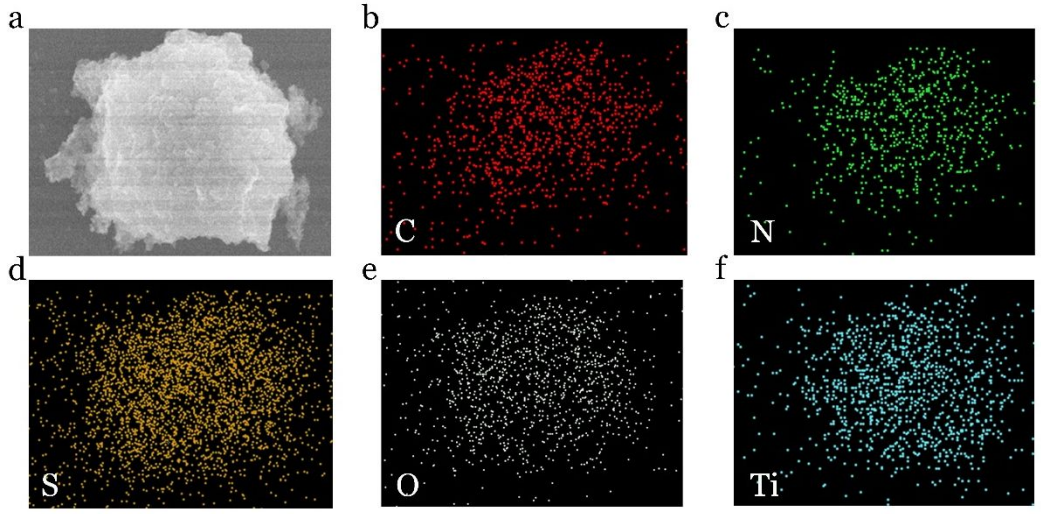

Figure S8. (a) SEM image of the HCPT@COF/S composite after sulfur infiltration. (b-f) Elemental maps of Carbon (b), Nitrogen (c), Sulfur (d), Oxygen (e) and Titanium (f).

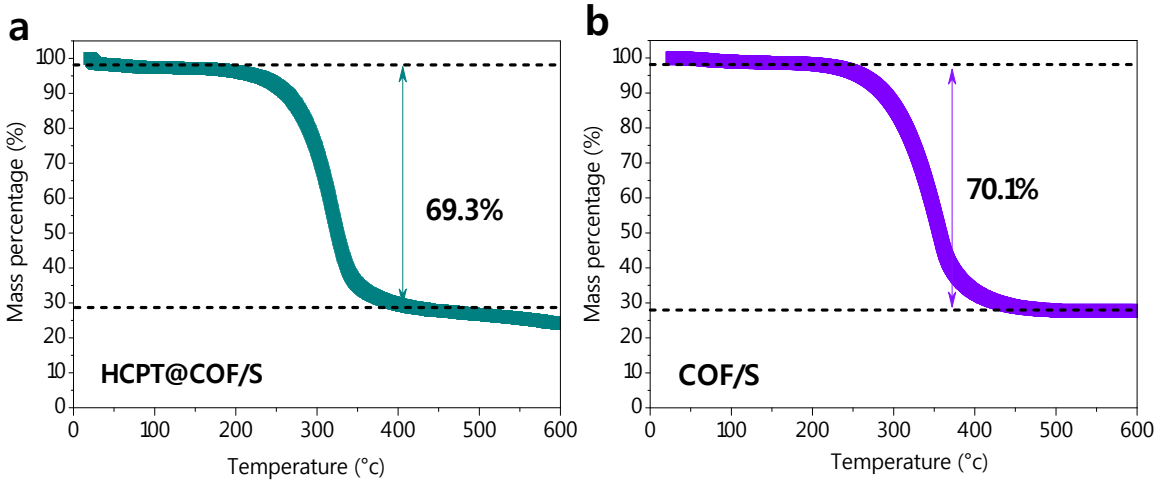

Figure S9. TGA results of the HCPT@COF/S (a) and COF/S (b).

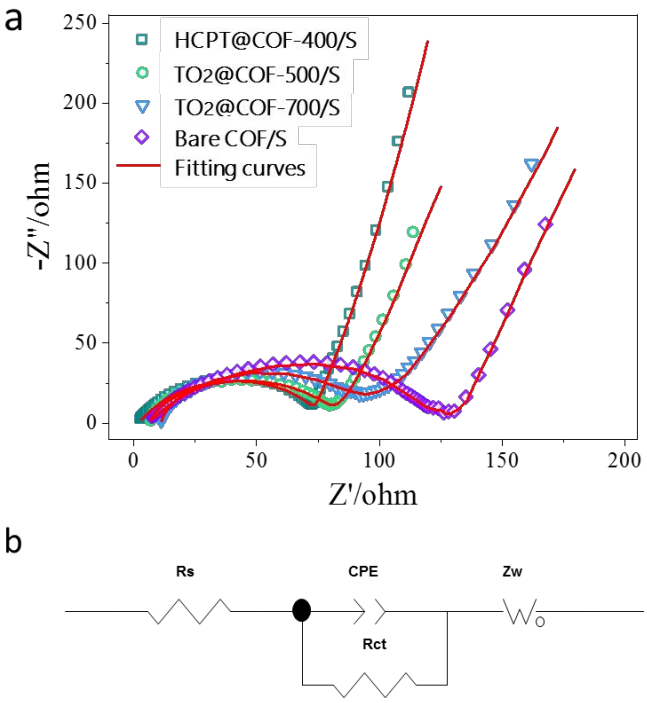

Figure S10. Nyquist plots (a) and equivalent circuit (b) of the COF/S electrode, and the HCPT@COF-400/S, TiO_2@COF-500/S and TiO_2@COF-700/S composite electrodes for Li-S batteries before cycling. R_s: contact resistance; R_{ct}: charge transfer resistance; *CPE*: constant phase element (space double-layer capacitance); Z_w: Warburg impedance.

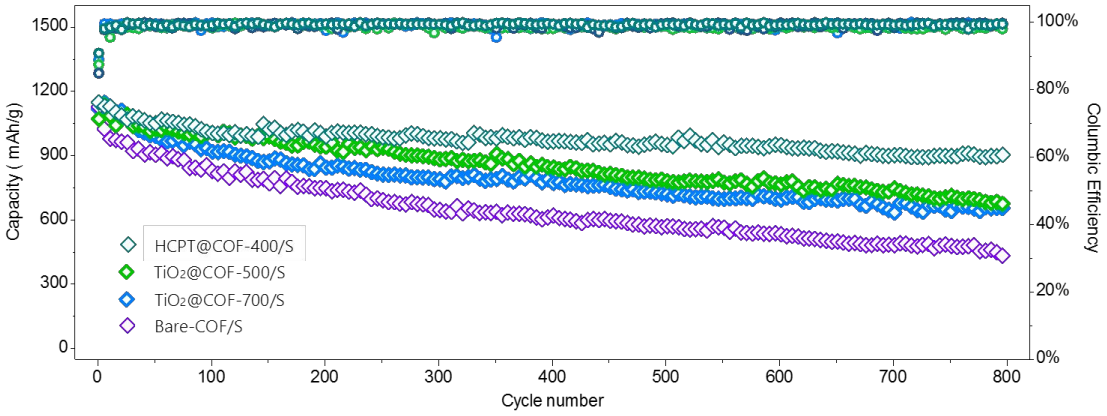

Figure S11. Cycling performance of the COF/S, HCPT@COF-400/S, TiO_2@COF-500/S, TiO_2@COF-700/S composite electrodes at 0.5 C.

Note: The cycling performance tests for the TiO_2@COF/S composites synthesized at higher temperatures display that the electrochemical performance decreases with increasing reaction temperatures: the specific capacity for the TiO_2@COF-500/S and TiO_2@COF-700/S composite electrodes reached 700.2 and 652.9 mAh/g respectively at 800^{th} cycle.

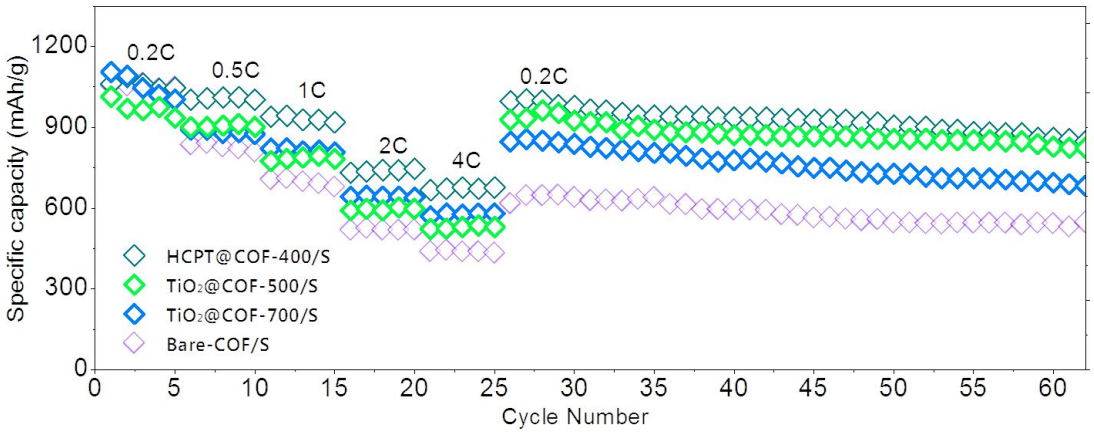

Figure S12. Rate performance of the COF/S, HCPT@COF-400/S, TiO_2@COF-500/S, TiO_2@COF-700/S composite electrodes at variable current density of 0.2, 0.5, 1, 2 and 4 C.

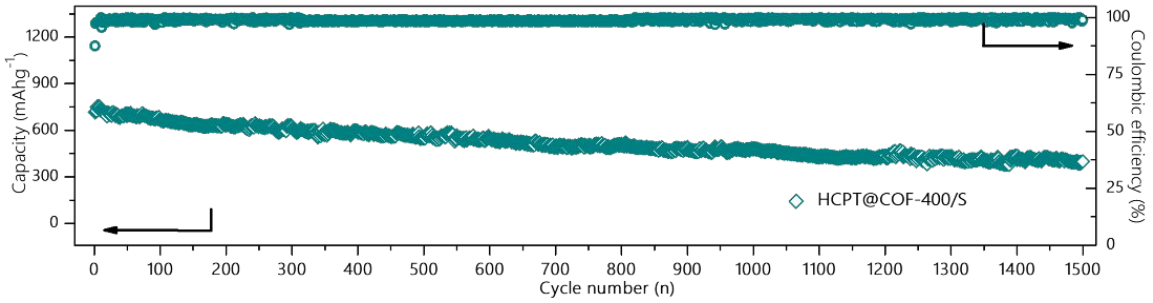

Figure S13. Cycling performance of the HCPT@COF-400/S composite electrode at 3 C.

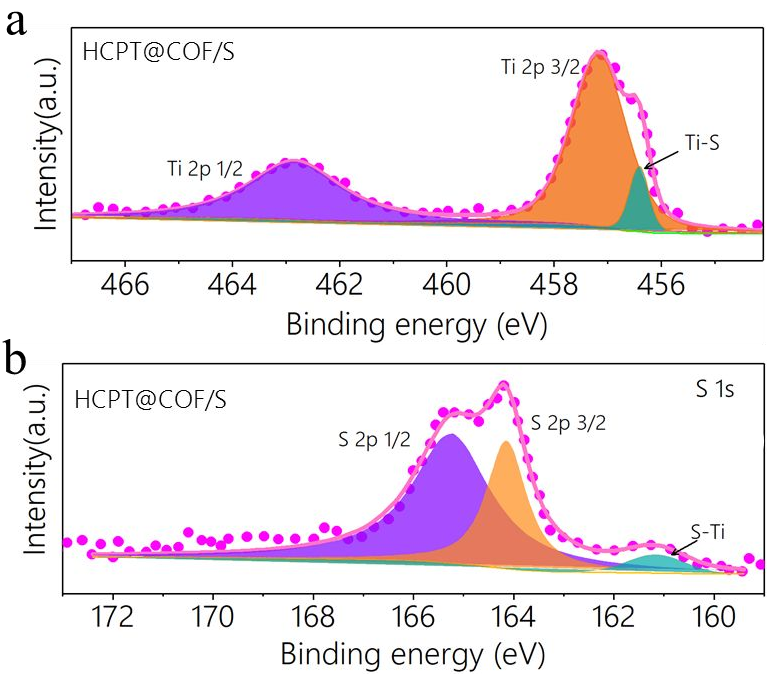

Figure S14. X-ray photoelectron spectra of the HCPT@COF/S composite electrode. a) Ti *2p*. b) S *2p*.

Note: In Figure S14 a, the as-synthesized HCPT@COF/S composite exhibits a new Ti $2p^{3/2}$ peak at 456.7 eV, which corresponds to the formation of S-Ti bond.[1,2] Figure S14 b shows two typical sulfur characteristic peaks at 165.8 eV and 164.2 eV, with the additional peak at 161.3 eV confirming the existence of S-Ti bond in the HCPT@COF/S composite.

2

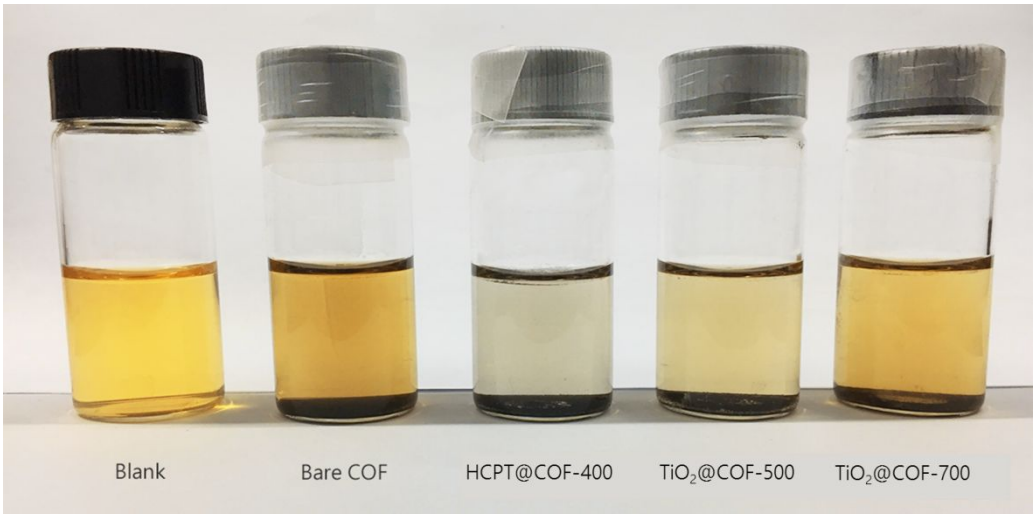

Figure S15. A digital photograph of 0.05 mol/L brownish yellow Li_2S_6 solution absorption experiment with the addition of (from left to right) the bare COF, and the HCPT@COF-400, TiO_2@COF-500 and TiO_2@COF-700 composites after 3 h.

Table S1. BET data of specific surface area and pore volume for the bare COF, and the HCPT@COF-400, TiO_2@COF-500 and TiO_2@COF-700 composites.

Sample	Bare COF	HCPT@COF-400	TiO_2 @ COF-500	TiO_2 @ COF-700
S_{BET} (m^2/g)	943	809	1043	1174
V_{pore} (cm^3/g)	0. 96	0. 87	0. 92	1. 63

Table S2. XPS elemental analysis of the HCPT@COF composite (HCPT@COF-400).

Peak	Type	Position BE (eV)	Atomic Conc %	Mass Conc %
O 1s	Reg	530.1	7.67	9.44
Ti 2p	Reg	458.9	1.36	5
N 1s	Reg	397.9	9.68	10.43
C 1s	Reg	284.4	81.29	75.12

Table S3. Impedance parameters calculated with the different TiO_2@COF-S electrode for Li-S battery

	R_s	*CPE*		R_{ct}	Z_w		
	(ohm)	*CPE-T*	*CPE-P*	*(ohm)*	*W-R*	*W-T*	*W-P*
Bare COF/S	6.22	3.1026E-5	0.69987	116.9	5.14	0.06144	0.39325
HCPT***@COF-400S***	2.389	1.4662E-5	0.7883	72.02	2.5	0.00106	0.43734
TiO_2@COF-500S	6.353	1.0443E-5	0.81538	68.28	28.39	0.034157	0.4143
TiO_2@COF-700S	9.7	4.4434E-6	0.86387	68.9	72	0.033	0.38

*R*s is the contact resistance. *R*ct is charge-transfer resistance. *CPE* is constant phase element (space double-layer capacitance). *Zw* is Warburg impedance.

Note S1. Method and Model of DFT calculations

The first principles calculations in the framework of density functional theory, including structural, electronic performances, were carried out based on the Cambridge Sequential Total Energy Package known as CASTEP [3]. The exchange–correlation functional under the generalized gradient approximation (GGA) [4] with norm-conserving pseudopotentials and Perdew–Burke–Ernzerhof functional was adopted to describe the electron–electron interaction.[5] An energy cutoff of 750 eV was used and a k-point sampling set of 5 × 5 × 1 were tested to be converged. A force tolerance of 0.01 eV $Å^{-1}$, energy tolerance of 5.0 × 10^{-7} eV per atom and maximum displacement of 5.0 × 10^{-4} Å were considered. Each atom in the storage models is allowed to relax to the minimum in the enthalpy without any constraints. The vacuum space along the z direction is set to be 15 Å.

References

(1) Zang, X.; Shen, C.; Kao, E.; Warren, R.; Zhang, R.; Teh, K.; Zhong, J.; Wei, M.; Li, B.; Chu, Y.; Sanghadasa, M.; Schwartzberg, A.; Lin, L. Titanium disulfide coated carbon nanotube hybrid electrodes enable high energy density symmetric pseudocapacitors. *Adv. Mater.* **2017**, *30*, 1704754.

(2) Bao, W.; Lin, L.; Wang, C.; Choi, S.; Dan, W.; Wang, G. Facile synthesis of crumpled nitrogen-doped MXene nanosheets as a new sulfur host for lithium–sulfur batteries. *Adv. Energy Mater.* **2018**, *8*, 1702485.

(3) Segall, M. D.; Probert, P. J. D. L. M. J.; Pickard, C. J.; Hasnip, P. J.; Clark, S. J.; Payne, M. C. First-principles simulation: ideas, illustrations and the CASTEP code. *J. Phys.: Condens. Matter* **2002**, *14*, 2717.

(4) Perdew, J. P.; Burke, K.; Ernzerhof, M. Generalized gradient approximation made simple. *Phys. Rev. Lett.* **1996**, *77*, 3865.

(5) Hamann, D. R.; Schlüter, M.; Chiang, C. Norm-conserving pseudopotentials. *Phys. Rev. Lett.* **1979**, *43*, 1494.